Chapter 14
BCS–BEC Crossover and Unconventional Superfluid Order in One Dimension

A. E. Feiguin, F. Heidrich-Meisner, G. Orso and W. Zwerger

Abstract In this chapter we discuss the BCS–BEC crossover in one-dimensional Fermi gases. We present exact results using the Bethe Ansatz as well as numerical calculations of the correlation functions and the complete phase diagram. In a balanced gas, a continuous crossover occurs from a BCS-type fermionic superfluid to a BEC of pairs that are described by the Lieb-Liniger model. In the case of a finite imbalance, superfluidity persists in the form of a Fulde-Ferrell-Larkin-Ovchinnikov (FFLO) state with finite-momentum pairs on the weak coupling side. For strong attractive interactions, it is replaced by a Bose-Fermi mixture. The perspectives to observe an FFLO-state with ultracold fermions in a harmonic trap are discussed.

A. E. Feiguin
Department of Physics and Astronomy,
University of Wyoming,
Laramie, WY 82071,
USA
e-mail: afeiguin@uwyo.edu

F. Heidrich-Meisner · G. Orso
Department of Physics,
Arnold Sommerfeld Center for Theoretical Physics,
Ludwig-Maximilians-Universität München,
D-80333 München,
Germany
e-mail: heidrich-meisner@lmu.de

G. Orso
e-mail: giuliano.orso@univ-paris-diderot.fr

W. Zwerger
Physik Department, Technische Universität München,
D-85747 Garching,
Germany
e-mail: zwerger@ph.tum.de

W. Zwerger (ed.), *The BCS–BEC Crossover and the Unitary Fermi Gas*,
Lecture Notes in Physics 836, DOI: 10.1007/978-3-642-21978-8_14,

14.1 Introduction

Starting with the historic controversy between Bardeen and Schafroth about the proper explanation of superconductivity, the crossover from a Bardeen–Cooper–Schrieffer (BCS) superfluid with Cooper pairs, whose size is much larger than the inter-particle spacing, to a Bose–Einstein Condensate (BEC) of molecules composed of fermions tightly bound into pairs has been a fundamental issue in many-body physics. The realization of fermionic superfluids with ultracold gases near a Feshbach resonance has turned this more or less academic, fifty-year-old problem into one that can be studied experimentally [1–3]. In the 3D situation, the crossover is well understood for the balanced gas, despite the fact that no analytical results are available for even the most basic quantities such as the ground-state energy or the critical temperature of the superfluid to normal gas transition in the most interesting regime near unitarity. In the situation with a finite imbalance, many questions are still open, in particular, the issue of unconventional superfluids that are expected in some parts of the phase diagram (see the chapters by Bulgac, Forbes and Magierski, by Diederix and Stoof and by Recati and Stringari). It is therefore of considerable interest to have an analytically solvable model of the BCS–BEC crossover that provides quantitative results in a particular case and, moreover, a better understanding of the conditions under which unconventional superfluid pairing may appear. Such an exact solution of the problem is possible in one dimension (1D), both for the balanced [4, 5] and the imbalanced gas [6, 7]. The importance of this solution goes beyond the generic interest in solvable many-body problems because

1. 1D Fermi gases with a tunable attractive interaction and arbitrary values of the imbalance have been realized experimentally [8, 9] and
2. the imbalanced 1D Fermi gas exhibits unconventional superfluid order of the FFLO type [10, 11] in a wide range of the phase diagram [12–19].

In the FFLO state, the pairs that form the superfluid acquire a finite center-of-mass momentum and thus lead to an order parameter that oscillates in real space. Such an unconventional superfluid has been predicted by Fulde and Ferrell [10] and—in a more general form—by Larkin and Ovchinnikov [11]. Despite intense research over several decades, this state has never been seen unambiguously, neither in condensed matter nor in the more exotic context of QCD at high densities, where FFLO-type phases based on pairing of quarks are predicted [20]. There is only some indirect evidence for an FFLO state from specific heat data on organic superconductors in a very strong magnetic field parallel to the layer structure [21]. As will be shown below, ultracold Fermi gases in 1D with a finite imbalance provide a rather simple realization of a state with finite-momentum Cooper pairs and thus give rise to the hope that this elusive unconventional superfluid can eventually be observed experimentally.

This chapter provides an introduction to FFLO-physics in one dimension and to exactly solvable 1D Fermi gases with attractive interactions in general (see also the recent reviews by Sheehy and Radzihovsky [22, 23]).

14.2 BCS–BEC Crossover of a Balanced One-Dimensional Fermi Gas

In a 3D gas, the BCS–BEC crossover is realized by changing the attractive contact interaction between two different hyperfine states through a Feshbach resonance, beyond which a bound state appears in the two-particle problem in free space. On the BCS side of the crossover, pairs only exist in the many-body system due to the Pauli blocking of states below the Fermi energy, which gives rise to a finite density of states at effectively zero energy. In one and also in two dimensions, the situation is quite different because any purely attractive interaction produces a bound state already at the two particle level. In fact, the existence of a two-body bound state is both a necessary and sufficient condition for a BCS instability [24]. At first sight, this seems to exclude a crossover with a proper BCS-limit in 1D because a two-body bound state is always present. Moreover, the BEC limit of tightly bound pairs is very special in 1D, because the Pauli principle for the constituent fermions makes these pairs behave like hard-core bosons. The bound pairs thus form a strongly interacting Tonks–Girardeau gas, very different from the weakly interacting gas of dimers that appears on the BEC side of the crossover in 3D. Remarkably, the situation in a real physical context, where atoms are confined to individual 'quantum wires' of finite width $\ell_\perp$ by, e.g., a strong 2D optical lattice, is different. In this case, an analog of the 3D crossover can be achieved in 1D by exploiting a confinement induced resonance (CIR) in a tight trap where the effective 1D scattering length exhibits a resonance caused by the mixing with a closed-channel bound state in the trap [25].

The microscopic Hamiltonian that describes a Fermi gas with two different components is the Gaudin–Yang (GY) model [26, 27]

$$H = -\frac{\hbar^2}{2m}\left(\sum_{i=1}^{N_\uparrow}\frac{\partial^2}{\partial x_i^2}+\sum_{j=1}^{N_\downarrow}\frac{\partial^2}{\partial y_j^2}\right)+g_1\sum_{i,\,j=1}^{N_\uparrow,\,N_\downarrow}\delta(x_i-y_j). \tag{14.1}$$

Here, x_i and y_j denote the coordinates of up- and down-spin fermions respectively, whose total numbers $N_\uparrow$, $N_\downarrow$ are fixed but, in general, different. The interaction between fermions of opposite spin is described by a contact potential $g_1\delta(x-y)$. Note that fermions of the same spin, which are never at the same point in space, have no interaction whatsoever in this model. In a situation where the atoms are subject to a transverse confinement, the strictly 1D model (14.1) is applicable provided that only the lowest eigenstate of the quantized motion in the transverse direction is occupied. For a harmonic confinement with radial frequency $\omega_\perp/2\pi$ and associated oscillator length $\ell_\perp=\sqrt{\hbar/m\omega_\perp}$, this requires $\varepsilon_F \ll \hbar\omega_\perp$ or—equivalently— $n\ell_\perp \ll 1$, where $n \equiv N/L$ is the 1D density at total particle number $N = N_\uparrow + N_\downarrow$. In this low density regime, the replacement of the actual interaction between ultracold atoms by a 1D contact potential turns out to be valid over a rather wide range of coupling constants. Indeed, the momenta for the scattering of two fermions are of the order of the Fermi momentum $k_F = \pi n/2$. The reflection amplitude

$$f(k) = \frac{-1}{1 + i\cot(\delta(k))} \simeq \frac{-1}{1 + ika_1 + \mathcal{O}\left((k\ell_\perp)^3\right)} \tag{14.2}$$

that describes two-particle scattering in 1D [1] can thus be replaced by its low-energy limit $-1/(1 + ika_1)$ as long as $k_F^2 \ll a_1/\ell_\perp^3$. Here, a_1 is the 1D scattering length, which is the single parameter that describes low-energy scattering in 1D. For a δ-function potential $V(x) = g_1\delta(x)$, the low-energy expression $-1/(1 + ika_1)$ for the reflection amplitude holds for arbitrary k, with scattering length $a_1 = -2\hbar^2/mg_1$, which is positive for attractive interactions $g_1 < 0$. The replacement of the actual inter-atomic potential by an effective contact interaction in 1D thus requires the density to be small enough such that the condition $(n\ell_\perp)^2 \ll a_1/\ell_\perp$ is obeyed. Since $n\ell_\perp \ll 1$ in the single transverse mode limit, this condition is satisfied in a rather wide range, except very close to the confinement induced resonance, where a_1 vanishes (see Eq. 14.4).

In the case of a uniform, balanced gas with total density n, the Hamiltonian (14.1) is characterized by a single dimensionless coupling constant $\gamma \equiv mg_1/\hbar^2 n$, which is inversely proportional to the density. In 1D, the strong coupling limit $|\gamma| \gg 1$ is therefore reached at *low* densities. This initially counterintuitive fact can be understood by noting that low densities imply small momenta. Moreover, the 1D scattering amplitude (14.2) has its maximum phase shift $\delta(0) = \pi/2$ as $k \to 0$ because 1D potentials become impenetrable at zero energy, i.e. $f(k \to 0) = -1$. At low densities, therefore, the interaction is strongest, quite in contrast to the 3D case where the s-wave phase shift $\tan\delta_0(k) = -ka + \ldots$ vanishes in the low-energy limit. The dimensionless coupling constant $\gamma = -\pi/(k_F a_1)$ is therefore large when the 1D scattering length is much smaller than the Fermi wave-length.

For weak attractive interactions $\gamma \to 0^-$, the ground state of the Gaudin–Yang model in the balanced case $N_\uparrow = N_\downarrow$ is a BCS-like state with Cooper pairs, whose size is much larger than the average inter-particle spacing. This is a direct consequence of the fact that the binding energy of these pairs (or—more precisely—the so called spin gap that separates the singlet ground state from the first triplet excited state) [4]

$$\Delta = \varepsilon_F \cdot \frac{16}{\pi}\sqrt{\frac{|\gamma|}{\pi}}e^{-\pi^2/2|\gamma|} \tag{14.3}$$

is much smaller than the Fermi energy ε_F in the weak coupling limit $k_F a_1 \gg 1$. At a given strength a_1 of the attractive interaction, this gap decreases exponentially as $\Delta \sim \exp(-\pi k_F a_1/2)$ with increasing density $n \sim k_F$, in contrast to the 3D case, where $\Delta \sim \exp(-\pi/2k_F|a|)$ strongly increases as the density and therefore, k_F grows. This fundamental difference is the basic reason for the fact that the unbalanced superfluid appears at the *edge* of a trapped gas with a finite overall imbalance and not in its center, as in 3D (see Sect. 14.3.2). The origin of this can be understood as a simple density-of-states effect. Indeed, the formation of pairs due to weak attractive interactions in a Fermi gas is favored by a large density of states $\nu(\varepsilon_F)$ at the Fermi energy. In 3D, $\nu_{3D}(\varepsilon_F) \sim \sqrt{\varepsilon_F} \sim k_F$ increases linearly with k_F while in 1D, due to $\nu_{1D}(\varepsilon_F) \sim 1/\sqrt{\varepsilon_F} \sim 1/k_F$, the situation is reversed and pairing is strong at *low*

densities. In the strong coupling regime $k_F a_1 \ll 1$, the attractive interaction leads to the formation of tightly bound molecules, whose binding energy coincides with the binding energy of the two-body problem $\Delta \equiv \varepsilon_b$. These pairs behave like a hard-core Bose gas. In a strictly 1D situation, therefore, the BEC limit of the crossover corresponds to a Tonks–Girardeau gas of dimers and one never reaches a weakly interacting BEC as in 3D.

A rather different situation, however, is encountered for the physically relevant case of 3D fermions that are confined in a quasi-1D geometry, such that their transverse degrees of freedom are completely frozen. For simplicity, we assume the atoms to be trapped in a harmonic waveguide with radial frequency $\omega_\perp/2\pi$ and oscillator length $\ell_\perp$. As shown by Bergeman et al. [28], the exact solution of the two-body scattering problem in such a waveguide always exhibits one and only one two-body bound state with energy $\tilde{\varepsilon}_b$, *whatever* the 3D scattering length a. Apart from this bound state, the low energy scattering properties can be described by an effective 1D delta potential $g_1\delta(x)$ with strength [25]

$$g_1(a) = \frac{2\hbar\omega_\perp a}{1 - Aa/\ell_\perp} \quad \leftrightarrow \quad \frac{a_1(a)}{\ell_\perp} = -\frac{\ell_\perp}{a} + A. \tag{14.4}$$

Here, $A = -\zeta(1/2)/\sqrt{2} \simeq 1.0326$ is a numerical constant. As naively expected, an attractive 3D interaction $a < 0$ implies a negative value of g_1. The associated two-particle bound state has energy $\varepsilon_b = mg_1^2/4\hbar^2$ and coincides with the exact bound state energy $\tilde{\varepsilon}_b$ in the limit $a/\ell_\perp \to 0$. Remarkably, g_1 and also the binding energy $\tilde{\varepsilon_b} = 0.606\hbar\omega_\perp$ remain finite at a Feshbach resonance $a = \pm\infty$, a prediction that has been verified experimentally [9]. Entering the positive side $a > 0$, the vanishing of the 1D scattering length a_1 at $\ell_\perp/a = A \simeq 1.0326$ leads to a CIR, where g_1 jumps from $-\infty$ to $+\infty$ just as in a standard 3D Feshbach resonance. For $g_1 > 0$, the short-range potential $g_1\delta(x)$ no longer has a bound state. It is still present, however, in the quasi-1D problem and its energy $\tilde{\varepsilon}_b$ is always larger than its value $2\hbar\omega_\perp$ at the CIR [28].

For a 1D gas with a finite density, the condition that only the lowest eigenstate of the transverse motion is occupied requires $\hbar\omega_\perp$ to be much larger than the Fermi energy ε_F. Beyond the CIR at $1/\gamma = 0$, the true bound-state energy $\tilde{\varepsilon}_b \geq 2\hbar\omega_\perp$ is therefore the largest energy scale in the problem and the dimers in this regime are essentially unbreakable bosons. In order to describe the resulting 1D Bose gas, one needs to know the effective interaction between these composite bosons. This has been studied by Mora et al. [29], who have solved the four-body scattering problem in 1D with delta-function interactions between the particles in the presence of a harmonic, transverse confinement. It turns out that the effective interaction of the dimers can again be described by a pseudo-potential $g_{dd}\delta(x)$, with a *repulsive* interaction constant $g_{dd} > 0$. Far away from the CIR, were the dimer size $a \ll \ell_\perp$ is much smaller than the scale $\ell_\perp$ of the transverse confinement, this interaction coincides with that expected from the free space result for the dimer-dimer scattering length $a_{dd} \simeq 0.6a$ in 3D, which has been derived by Petrov et al. [30]. As a result, $g_{dd} \to 2\hbar\omega_\perp a_{dd}$ vanishes in the deep BEC limit $a \to 0$ and one recovers—as in

3D—a weakly interacting Bose gas of dimers. Close to the resonance, the effective g_{dd} diverges, consistent with the expectation that the dimers near the CIR form a Tonks–Girardeau gas of hard-core bosons. In a waveguide geometry, therefore, there is a full BCS–BEC crossover in one dimension [4, 5] that is described by a Gaudin–Yang model of attractively interacting fermions up to the CIR and a Lieb–Liniger model [31] of repulsive bosons beyond the CIR. On a formal level, the continuous evolution from an attractive Fermi to a repulsive Bose gas in one dimension is implicit in the Bethe-ansatz equations of these models, as noted already by Gaudin [26]. Indeed, the ground-state energy per particle

$$\frac{E_0}{N} = \frac{\varepsilon_b}{2} + 2\int_{-B}^{B} \frac{d\lambda}{n}\sigma(\lambda)\frac{\hbar^2\lambda^2}{2m} \tag{14.5}$$

of the attractive Fermi gas is obtained from the solution of the Bethe-ansatz integral equation

$$\pi\sigma(\lambda) = 1 + \int_{-B}^{B} \frac{dq}{n}\frac{\gamma\sigma(q)}{\gamma^2 + [(\lambda - q)/n]^2}. \tag{14.6}$$

Here, $\sigma(\lambda)$ is the distribution function of the quasi-momenta (rapidities). They appear in complex conjugate pairs $k^{\pm} = \lambda \pm i/a_1$ and describe the $N/2$ bound states of the balanced gas. The value of B is fixed by the normalization $\int_{-B}^{B} d\lambda\sigma(\lambda) = n/2$. For the fermionic Gaudin–Yang problem, γ is negative. Remarkably, the identical equation applies for the Lieb–Liniger gas of dimers, where γ is positive. Since one is now dealing with dimers of mass $2m$ and density $n/2$, the dimensionless parameter $\gamma = 4mg_{dd}/\hbar^2 n = -4/(na_{1,dd})$ depends on the coupling constant g_{dd} or the associated scattering length $a_{1,dd}$ of the dimer-dimer interaction. Its dependence on the experimentally accessible parameters a and $\ell_\perp$ is determined by the exact solution of the 1D dimer-dimer scattering problem in the presence of a transverse confinement by Mora et al. [29]. As a function of the experimentally tunable ratio $\ell_\perp/a$, the resulting parameter $1/\gamma$, which replaces the standard inverse coupling constant $1/k_F a$ for the 3D crossover problem, smoothly grows from $1/\gamma = 0$ at the CIR $a \simeq \ell_\perp$ to $1/\gamma \gg 1$ in the BEC limit $a \ll \ell_\perp$, where the size of the dimers is much smaller than the transverse confinement length. More precisely, the effective dimer-dimer interaction g_{dd} that determines the dimensionless coupling constant $\gamma > 0$ on the BEC-side, does not diverge at the CIR of the atoms but close to the 3D Feshbach resonance, where the exact two-particle binding energy is close to $\tilde{\varepsilon_b} \simeq 0.6\hbar\omega_\perp$, see Fig. 1 in [29].

The qualitative physics of the BCS–BEC crossover in a balanced 1D Fermi gas is now easy to understand: in the high-density, BCS limit $-\pi/\gamma = k_F a_1 \gg 1$, the system consists of weakly bound Cooper pairs. In this regime, there is a gap between the singlet ground state and the first excited triplet state that increases strongly with decreasing density. In addition, there are gapless density fluctuations, describing

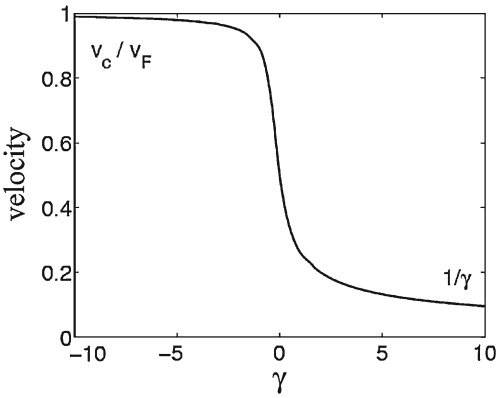

Fig. 14.1 Velocity of the Bogoliubov sound mode along the 1D BCS–BEC crossover

the Bogoliubov-Anderson mode of a neutral superfluid. The attractive Fermi gas is thus a so called Luther-Emery liquid [32, 33]. At the confinement induced resonance, when $k_F a_1 = 0$, the system is a Tonks–Girardeau gas of tightly bound dimers. It still exhibits sound modes with a linear spectrum, however, the spin excitations have disappeared because the spin gap is effectively infinite. For positive 3D scattering lengths $0 < a \simeq \ell_\perp$, the system is an interacting Bose gas of tightly bound molecules. Its excitations are the standard Bogoliubov sound modes, whose velocity vanishes asymptotically in the weak coupling (BEC) limit $1/\gamma \gg 1$, as shown in Fig. 14.1. The possibility of separating the BCS–BEC crossover into a purely fermionic problem on one side of the CIR and a purely bosonic one on the other side of the resonance is a peculiar property of one dimension. It relies on the assumption of a dilute system $n\ell_\perp \ll 1$, whose Fermi energy is much smaller than the binding energy at resonance. Defining a characteristic length scale $r^\star$ by the two-particle binding energy $\varepsilon^\star = \hbar^2/m(r^\star)^2$ at resonance, the low density condition $k_F r^\star \ll 1$ in 1D is completely equivalent to the condition $k_F r^\star \ll 1$ of a broad Feshbach resonance in 3D [1]. In this form, the condition applies more generally also for a two-channel, Bose-Fermi resonance model [34]. In the opposite, narrow Feshbach resonance limit $k_F r^\star \gg 1$, the physics near the CIR becomes more complicated. In particular, a new phase appears where atoms and dimers, both in a superfluid state with algebraically decaying correlations, coexist [35, 36].

14.3 Spin-Imbalanced Fermi Gas in One Dimension

In this section we discuss the extension of the Gaudin–Yang solution for a balanced attractive Fermi gas to the situation with a finite imbalance, as presented in [6, 7]. We first discuss the quantum phase diagram for the homogeneous system, where the underlying model is integrable by means of the Bethe ansatz. We then include a longitudinal trapping potential via the local density approximation and derive the

shell-structure of the density profiles of the two components. Effects of finite temperature have been investigated using the Bethe ansatz in [37, 38] and will not be covered here. A similar behavior at zero temperature is found for the case of optical lattices at filling factors below one. This case is covered in [39].

14.3.1 Bethe-Ansatz Solution for the Homogeneous Gas

The Hamiltonian (14.1) can be diagonalized exactly also in the presence of a finite spin polarization. For fixed values of the linear number densities $n_\uparrow = N_\uparrow/L$ and $n_\downarrow = N_\downarrow/L$, where L is the size of the system, the ground state energy E is given by

$$\frac{E}{L} = \frac{4\hbar^2}{ma_1^3}\left[\int_{-B}^{B}\left(2\lambda^2 - \frac{1}{2}\right)\sigma(\lambda)\mathrm{d}\lambda + \int_{-Q}^{Q} k^2\rho(k)\mathrm{d}k\right], \tag{14.7}$$

where $a_1 = -2\hbar^2/mg_1$ is the effective 1D scattering length, and B and Q are non-negative numbers related to the particle densities by $n_\downarrow a_1 = 2\int_{-B}^{B}\sigma(\lambda)d\lambda$ and $n_\uparrow a_1 - n_\downarrow a_1 = 2\int_{-Q}^{Q}\rho(k)dk$. The spectral functions $\sigma(\lambda)$ and $\rho(k)$ appearing in Eq. 14.7 are solutions of two coupled integral equations [26]

$$\sigma(\lambda) = \frac{1}{\pi} - \int_{-B}^{B} K_1(\lambda,\lambda')\sigma(\lambda')d\lambda' - \int_{-Q}^{Q} K_2(\lambda,k)\rho(k)dk,$$

$$\rho(k) = \frac{1}{2\pi} - \int_{-B}^{B} K_2(\lambda,k)\sigma(\lambda)d\lambda, \tag{14.8}$$

where the kernels are given by $\pi K_1(\lambda,\lambda') = 1/[1 + (\lambda' - \lambda)^2]$ and $\pi K_2(\lambda,k) = 2/[1 + 4(k - \lambda)^2]$. The need for a second distribution function $\rho(k)$ beyond the function $\sigma(\lambda)$ introduced in Sect. 14.1 for the balanced gas is due to the presence of uncompensated spins in the imbalanced case $n_\uparrow \neq n_\downarrow$. These uncompensated spins are not bound in pairs and are thus described by real rapidities k_j. In the thermodynamic limit, this gives rise to a distribution function $\rho(k)$. It is only for $n_\uparrow = n_\downarrow$ that no uncompensated spins exist. In this case, we have $Q = 0$ and the coupled set of equations (14.8) reduces to a single integral equation for $\sigma(\lambda)$ which is identical to Eq. 14.6 discussed in Sect. 14.1 by a trivial rescaling.

For a fixed value of the total density $n \equiv n_\uparrow + n_\downarrow$, the density difference $s \equiv n_\uparrow - n_\downarrow$ can vary in the range $0 \leq s \leq n$. For $s = 0$, the ground state of the Hamiltonian (14.1) is *fully paired* with a spin gap Δ, corresponding to the energy needed to break a pair in the many-body system, whereas in the opposite limit $s = n$,

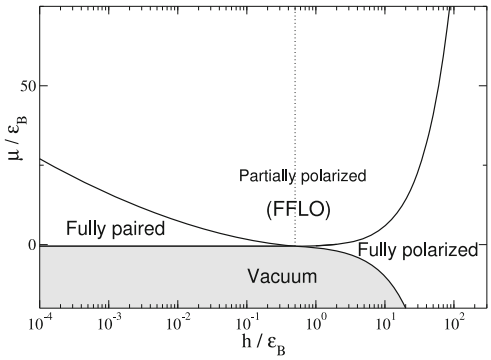

Fig. 14.2 Quantum phase diagram of attractively interacting fermions obtained from the Bethe-ansatz solution of the Gaudin model. Here $\mu, h = (\mu_\uparrow \pm \mu_\downarrow)/2$, where $\mu_{\uparrow,\downarrow}$ are the chemical potentials of the two components, and ε_b is the binding energy of the pair. Reproduced from [7]

the system is a *fully polarized* gas of $\uparrow$ fermions. For $0 < s < n$, the gas is *partially polarized* and is a superfluid of the FFLO type [12–19].

Using the mean chemical potential μ and the *effective* magnetic field h, defined as

$$\mu = \frac{\partial(E/L)}{\partial n}, \quad h = \frac{\partial(E/L)}{\partial s} \tag{14.9}$$

as new independent variables, one obtains the universal phase diagram shown in Fig. 14.2, where $\varepsilon_b = \hbar^2/ma_1^2$ is the binding energy of the molecule.

The phase boundary $h = h_c(\mu)$ between the partially polarized and the fully paired regions is calculated by setting $s = 0$ in Eq. 14.9. We see that h_c is a *decreasing* function of the chemical potential, being exponentially small at large particle density and reaching its maximum value $h_c = \varepsilon_b/2$ in the zero density limit. This behavior can be understood by noticing that the critical magnetic field is related to the spin gap Δ of the *unpolarized* gas by $h_c = \Delta/2$, and therefore, it increases when one enters into the low density regime (μ decreases), where interaction effects become stronger. We emphasize that in higher dimensions the situation is completely reversed [40] (see also the discussion in the previous section).

The boundary $h = h_s(\mu)$ between the partially polarized and the fully polarized phases in Fig. 14.2 is obtained by setting $s = n$ in Eq. 14.9. This yields the implicit formula $h_s = 2\varepsilon_b[Q^2(1 - \arctan(2Q)/\pi) + (2Q - \arctan(2Q) + \pi)/4\pi]$, with $Q = \sqrt{(\mu + h_s)/2\varepsilon_b}$. The fully paired and fully polarized phases correspond, respectively, to the paramagnetic and ferromagnetic states of a superconductor in a magnetic field [41, 42].

The presence of a two-body bound state leads to a direct boundary $\mu = -\varepsilon_B/2$ between the fully paired phase and the vacuum. In the fully polarized phase the atom density vanishes in correspondence to $\mu_\uparrow = (\mu + h)/2 = 0$, as for the 3D case [40]. We stress that the partially polarized phase has no direct boundary with the vacuum,

implying the absence of n-body bound states with $n > 2$. This feature will change in the presence of a mass asymmetry, as we shall discuss in Sect. 14.5.

We see from Fig. 14.2 that the fully paired and fully polarized phases *cannot* coexist for a fixed value of the magnetic field. In particular, for $h < \varepsilon_b/2$, only the fully paired phase is allowed, whereas for $h > \varepsilon_b/2$, only the fully polarized phase can occur. This property determines the shell structure of a trapped gas, as we shall see next.

14.3.2 Phase Separation in a Trap

We now assume that particles are trapped longitudinally by a shallow harmonic potential $V_{ho}(z) = m\omega_z^2 z^2/2$, where ω_z is the trapping frequency, and we calculate the density profiles of the two components via the local density approximation (LDA). This is done by imposing the local equilibrium condition $\mu_\sigma[n_\uparrow(z), n_\downarrow(z)] + V_{ho}(z) = \mu_\sigma^0$, where $\mu_\sigma[n_\uparrow, n_\downarrow]$ are the corresponding chemical potentials of the homogeneous system and μ_σ^0 are constants fixed by the normalization $N_\sigma = \int n_\sigma(z)dz$. Taking into account that $\mu, h = (\mu_\uparrow \pm \mu_\downarrow)/2$, this reduces to

$$\begin{aligned} \mu[n_\uparrow(z), n_\downarrow(z)] &= \mu^0 - V_{ho}(z), \\ h[n_\uparrow(z), n_\downarrow(z)] &= h^0, \end{aligned} \tag{14.10}$$

where $\mu^0, h^0 = (\mu_\uparrow^0 \pm \mu_\downarrow^0)/2$. Equation 14.10 shows that the LDA trajectories correspond to vertical lines in the phase diagram of Fig. 14.2, implying that the trapped one-dimensional gas phase-separates into *two* shells: a partially polarized core and either fully paired or fully polarized wings. This is a key difference with respect to three-dimensional systems, where the trap induces a three-shell structure [40].

In Fig. 14.3 we show the calculated Thomas–Fermi radii R_{in} and $R_\uparrow$ of the inner and outer shells, respectively. These are plotted as a function of the spin polarization $P \equiv (N_\uparrow - N_\downarrow)/N$, where $N = N_\uparrow + N_\downarrow$ is the total number of particles, and for different values of the interaction parameter $\lambda = Na_1^2/a_z^2$. In the absence of interactions, we find $R_\uparrow$, $R_{in} = \sqrt{1 \pm P}a_z N^{1/2}$ which are monotonic functions of P (*top curves*). For finite attractive interactions, the two radii show instead a non-monotonic behavior as a function of P, signaling the appearance of fully paired wings at low polarizations. In particular, the cloud size ($R_\uparrow$) first decreases as P increases because the density profiles of majority and minority components must match at the edge of the cloud. Beyond a critical value $P = P_c$ of the spin polarization, the outer shell becomes fully polarized, implying that the cloud size must increase steadily for $P > P_c$, as shown in Fig. 14.3. The critical spin polarization P_c increases going towards the strongly interacting dilute regime, where it eventually saturates at $P_c(\lambda = 0) = 1/5$ (see [6, 7] for details).

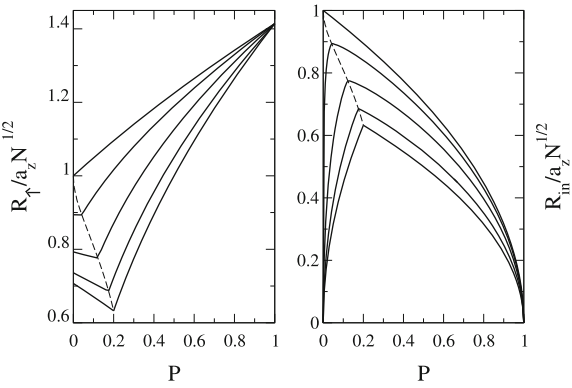

Fig. 14.3 Thomas–Fermi radii of the outer ($R_\uparrow$) and of the inner ($R_{\rm in}$) shell computed via LDA from the exact solution for the homogeneous system. Radii versus P for values of the interaction parameter $\lambda = \infty$, 10, 1, 0.1, 0 (*bottom to top*). The non-monotonic behavior is a signature of the fully paired wings at low spin polarization. Reproduced from [7] with permission of the author

14.4 FFLO Correlations in the Partially Polarized Phase

14.4.1 Predictions From Bosonization

So far, we have only discussed the thermodynamics of attractive 1D fermions at zero temperature. As shown in the previous section, this allows one to determine the density profiles of trapped gases within LDA. A detailed understanding of the order that is present in the balanced and imbalanced attractive Fermi gas, however, requires to calculate correlation functions. Of particular interest is the nature of superfluid order in the ground state. It follows from the pair correlation

$$\rho_{ij}^{\rm pair} = \left\langle c_{i,\uparrow}^\dagger c_{i,\downarrow}^\dagger c_{j,\uparrow} c_{j,\downarrow} \right\rangle, \tag{14.11}$$

which describes the tendency for singlet pairing as a function of separation $x = i - j$ (we use a continuum or discrete notation interchangeably, in particular since quantitative results for correlation functions at arbitrary distances require using a lattice model with discrete sites i, see the following section). In a standard singlet superconductor, the pair correlation function approaches a finite constant at large separation $x \to \infty$, which is proportional to the square of the gap parameter in weak coupling. In one dimension, long-range order is destroyed by quantum fluctuations even in the ground state and at most algebraically decaying correlations may exist. For the balanced gas, the correlation exponent Δ_{SS} for singlet pairing, defined by $\rho_{ij}^{\rm pair} \sim |i - j|^{-\Delta_{SS}}$, turns out to be the inverse $\Delta_{SS} = 1/K_c$ of the (charge) Luttinger exponent K_c [32]. For attractive interactions, this implies $\Delta_{SS} < 1$. The singlet pairing correlations thus decay very slowly. They are, in fact, the dominant correlations in the system, i.e., those with the smallest value of the correlation exponent Δ in the two-particle

channel. In the case with a finite imbalance $P \neq 0$, superfluid pairing still persists in the ground state, however it changes both its nature and also decays more quickly with distance. The fact that the nature of pairing is different can be understood most easily from a mean-field description of pairing in the weak coupling limit. At finite imbalance $P = (n_\uparrow - n_\downarrow)/n > 0$, the two components have different Fermi wave vectors $k_{F,\sigma} = \pi n_\sigma$. A BCS-instability of the free Fermi gas, which pairs an up-spin fermion with a down-spin one at opposite sides of the respective Fermi 'surfaces' will thus lead to pairs with a finite total momentum

$$Q = k_{F\uparrow} - k_{F\downarrow} = \pi n P. \tag{14.12}$$

This results in an oscillating superfluid correlation function of the form

$$|\rho_{ij}^{\text{pair}}| \propto |\cos(Qx)|/x^{\Delta(p)} \tag{14.13}$$

which is characteristic of states of the FFLO-type (sometimes also denoted LOFF in the literature) order. Fermionic superfluids with pairs that have a finite momentum in the ground state were initially suggested for superconductors in the presence of strong internal magnetic fields [10, 11]. In the present context of imbalanced Fermi gases, the Hamiltonian is time-reversal invariant. The ground state therefore necessarily has a vanishing net current. Pairs with net momentum Q and $-Q$ are thus equally probable and the superfluid order parameter is a real function $\sim \cos(Qx)$, up to an arbitrary overall phase. A peculiar feature of the situation in one dimension is the fact that FFLO-type order is the dominant correlation (i.e. the one with the smallest value of the correlation exponent Δ) at arbitrary polarizations $P > 0$, up to $P = 1$ where the system is a trivial fully polarized and non-interacting Fermi gas [13, 16, 17]. (for early mean-field studies, see [43, 44]).

A convenient method to calculate the long-distance behavior of correlations in 1D quantum liquids is bosonization [32]. The attractive Fermi gas in the presence of a finite effective field h that couples to the imbalance in a Zeeman-like form $H' = -h(N_\uparrow - N_\downarrow)$ can thus be reduced to a sine-Gordon model for the spin-density field $\phi_s(x)$ that determines the imbalance via $p(x) \sim \partial_x \phi_s(x)$ [12]. The imbalance remains zero up to a critical value $h_c = \Delta/2$ of the effective field that is determined by the spin gap Δ of the balanced gas. Beyond this critical field, a finite density $n_{sol} = n_\uparrow - n_\downarrow = Q/\pi$ of solitons arises in $\phi_s(x)$ where the superfluid order parameter changes by π at each soliton. The associated pair correlation function has the form given in Eq. 14.13 with a correlation exponent $\Delta_{SS}(p) = \Delta_{SS}(p=0) + 1/2$. It is larger than the one of the balanced gas by an additional contribution $1/2$ that arises from the fluctuations around the average periodic order of the soliton lattice [12]. The appearance of an order parameter that is periodic in space can be understood in simple physical terms by noting that the additional up-spins in the imbalanced gas prefer to sit at the zeroes of the order parameter (naively associated with a locally vanishing pairing gap), which are $1/n_{sol}$ apart on average. These results are supported by detailed numerical investigations of correlation functions in the attractive Hubbard model on a 1D lattice, using density matrix renormalization

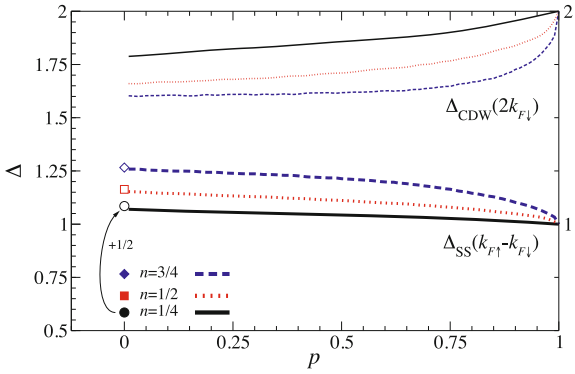

Fig. 14.4 Exponents of density-density correlations and (s-wave) pair-pair correlations functions, calculated numerically from the Bethe-ansatz, as a function of polarization and for several densities [16]

group (DMRG) or Quantum Monte Carlo (QMC) methods [12–19]. In particular, the values of the correlation exponents for density-density correlations (denoted by Δ_{CDW}) which are dominant for repulsive interactions and those for superfluid pairing of the FFLO-type are shown in Fig. 14.4. These results were obtained in [16] by numerically solving the respective Bethe-ansatz equations [45, 46]. It is evident that for attractive interactions, FFLO is the dominant instability at arbitrary values of the polarization, also compared to other algebraically decaying correlation functions such as, e.g., triplet superfluidity [16]. It is favored by small filling fractions on the lattice. Moreover, there is hardly any dependence of the exponents on polarization P beyond the initial jump by 1/2, in agreement with the predictions of bosonization. There is one major caveat, however, of this method, which will be discussed in the following.

The exact Bethe-ansatz solution of the imbalanced gas shows that the finite polarization $P(h) \sim (h - h_c)$ which appears beyond the critical field $h_c = \Delta/2$ starts *linearly* with the deviation from the critical field. By contrast, bosonization predicts a square root behavior $P(h) \sim \sqrt{h - h_c}$ of the polarization near the critical field [12]. This behavior is characteristic for the appearance of solitons in a Sine-Gordon model with a finite tilt, as was found by Pokrovsky and Talapov [47] in the context of 2D commensurate-incommensurate transitions. The failure of bosonization in this context has been discussed by a number of authors [48–51] and is due to a breakdown of spin-charge separation in this problem. To understand the physics behind this effect, it is convenient to consider the strong coupling limit $k_F a_1 \to 0^+$ of the attractive Fermi gas at given values of the total density n and density difference $s = n_\uparrow - n_\downarrow$. The ground-state is effectively a gas of dimers with density $n_d = n_\downarrow = (n - s)/2$ that coexists with a gas of unpaired fermions with density s. Since the dimers are hard-core bosons, the ground-state energy density is of the form [7]

$$e_0(n, s) = -\varepsilon_b n_d + e_0^{TG} + e_0^F = -\varepsilon_b n_d + \frac{\hbar^2\pi^2}{12m}\frac{1}{8}(n - s)^3 + \frac{\hbar^2\pi^2}{6m}s^3. \qquad (14.14)$$

Here e_0^{TG} is the energy density of the Tonks–Girardeau gas of dimers with mass $2m$ while e_0^F is that of a free Fermi gas. Note that there is no contribution $g_{ad} n_d s$ from the

atom-dimer repulsion here, because in one dimension the effective coupling constant g_{ad} turns out to vanish like s^2 [52]. Using $h = \partial e_0/\partial s$ and the strong coupling result $2h_c(n) = \varepsilon_b - \varepsilon_F/2 + \ldots$ for the critical field, Eq. 14.14 leads to

$$h - h_c = \frac{\varepsilon_F}{2} P - \frac{\varepsilon_F}{4} P^2 + 4\varepsilon_F P^2 + \ldots . \tag{14.15}$$

As a result, the dimensionless polarization $P = 2(h - h_c)/\varepsilon_F + \ldots$ vanishes linearly with $h - h_c$, consistent with the Bethe-ansatz solution (see also [50, 53]). The linear behavior is a result of a contribution $\varepsilon_F P^2/4$ to the ground-state energy density e_0^{TG} of the Tonks–Girardeau gas in Eq. 14.14. For small polarization $P \to 0$, this term dominates the kinetic energy $e_0^F \sim P^3$ of the Fermi gas of unpaired atoms that gives rise to the last, irrelevant contribution on the rhs of Eq. 14.15. The failure of bosonization is that it does not account for the change in the energy density e_0^{TG} that is associated with the creation of unpaired fermions from the gas of bound pairs. Bosonization pretends they are created out of a vacuum state whose energy is unaffected by a finite polarization. Only the kinetic energy $\sim P^3$ due to the filling of an initially empty band in the spin sector is included. A different way to see that bosonization cannot describe the correct linear dependence $P(h) = 2(h - h_c)/\varepsilon_F + \ldots$ is that it does not account for an energy scale of order ε_F, 'knowing' only about the Fermi momentum, which is proportional to $\sqrt{\varepsilon_F}$. Also note that the coupling between spin and charge that results from the nontrivial dependence of e_0^{TG} on n and s changes the effective interaction between individual unpaired fermions (i.e., the solitons of the Sine-Gordon theory) from the standard $1/x^3$-behavior discussed in the context of 2D commensurate-incommensurate transitions [47] to a longer range $1/x^2$-dependence.

14.4.2 Exact Numerical Results

In this section we wish to demonstrate that the FFLO correlations predicted from bosonization [12] indeed exist in the partially polarized phase of 1D systems of attractively interacting fermions. While both the Gaudin–Yang and the 1D Hubbard model, the lattice version, are integrable models, the calculation of correlation functions is notoriously difficult, and one therefore has to resort to numerically exact methods such as DMRG or QMC.

For concreteness, we consider the 1D attractive Hubbard model:

$$H_0 = -t \sum_{i=1,\sigma}^{L-1} \left(c_{i\sigma}^\dagger c_{i+1\sigma} + h.c. \right) + U \sum_{i=1}^{L} n_{i\uparrow} n_{i\downarrow} \tag{14.16}$$

with an attractive onsite interaction U and open boundary conditions. Here $c_{i\sigma}$ annihilates a fermion with spin σ at site i and $n_{i\sigma}$ is the local density of the fermions with spin σ. The phase diagram for the 1D attractive Hubbard model for $n \leq 1$ has the

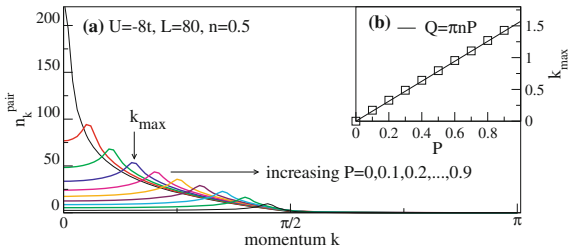

Fig. 14.5 Momentum distribution function of pairs in the 1D Hubbard model with $U = -8t$ and $n = 0.5$. In Eq. 14.18, $i_0 = L/2$. Inset: the position of the maximum in n_k^{pair} shows the expected scaling with $Q = k_{F\uparrow} - k_{F\downarrow} = \pi n P$. Compare also [14, 17] for the case of optical lattices and [15] for the case of the continuum

same phases as the continuum model: vacuum, partially polarized phase, fully paired phase, fully polarized phase [39, 54]. Additional phases emerge at larger densities that, however, are related to the aforementioned ones by means of a particle-hole transformation.

We use DMRG [55, 56] to compute the pair-pair correlation functions Eq. 14.11 [13, 17, 18]. Similar results can be obtained with QMC for both optical lattices [14] (there, the particle numbers are smaller than what can be accessed with DMRG [39], though) and the continuum case [15].

It is illustrative to go to momentum space by computing the associated momentum distribution function:

$$n_k^{\text{pair}} = (1/L) \sum_{lm} \exp[ik(l-m)] \rho_{lm}^{\text{pair}}. \tag{14.17}$$

Typical results for a homogeneous system with open boundary conditions are shown in the main panel of Fig. 14.5. At zero polarization $P = 0$, the MDF has a maximum at zero momentum, which, upon polarizing the system, shifts to finite momenta. The smoking gun for the presence of FFLO correlations is the scaling of the position Q of the finite-momentum maximum with polarization: in the case of 1D we expect Eq. 14.12 to hold. This is verified in the inset of Fig. 14.5, where we find $Q = \pi n P$, as expected (compare [13–15, 17, 18]). Note that this behavior is seen up to full polarization.

The next questions to address are the actual functional form of the spatial decay of pair correlations and the stability of FFLO correlations in the presence of a harmonic trap. We address both points by considering a trapped system

$$H = H_0 + V \sum_i n_i (i - i_0)^2, \tag{14.18}$$

summarizing key results from [13, 39] (see also [15, 18, 57]).

In Sect. 14.3, we emphasized that in the case of one dimension, the partially polarized phase always (i.e., at all U and $P > 0$) sits in the core of a trapped two-component Fermi gas, which can be predicted by applying LDA to the exactly known

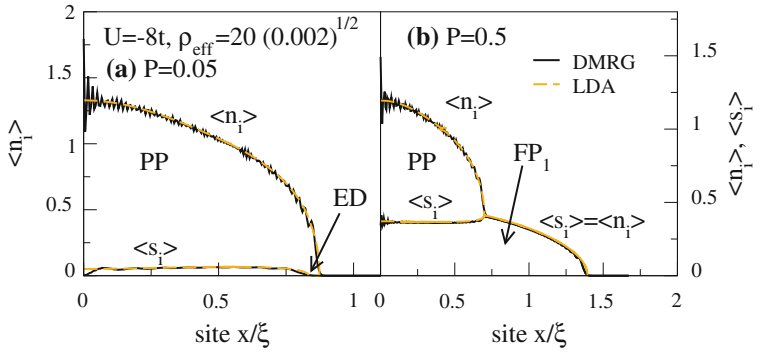

Fig. 14.6 Phase separation in an optical lattice with $U = -8t$, $N = 160$ fermions and (a) $P = 0.05$ and (b) $P = 1/2$ (reproduced from [39] with permission from the authors). Solid lines are DMRG results, dashed lines are LDA. If the main interest is in the behavior in the wings of a trapped Fermi gas, then it is computationally advantageous to use $i_0 = 0$ in Eq. 14.18 [39]

phase diagram of either the continuum [6, 7] or the lattice case [39]. This prediction was verified by exact numerical DMRG results in the case of an optical lattice [13, 18] and QMC simulations for the continuum [15] case. For illustration, we show DMRG results for the particle and the spin density profiles of a trapped Fermi gas at small polarizations $P < P_c$ and large polarizations $P > P_c$ in Fig. 14.6 [39], for which we have numerically obtained the ground-state of Eq. 14.18 with H_0 from Eq. 14.16 and realistic particle numbers of $N = 160$. Note that we display the spatial coordinate in units of the oscillator length $\xi = 1/\sqrt{V}$. Figure 14.6 clearly shows that the core is partially polarized and that the wings are fully paired for $P < P_c$ and fully polarized for $P > P_c$. Furthermore, for this particle number, the corresponding LDA result obtained from the exact Bethe-ansatz solution for the 1D attractive Hubbard model agrees quantitatively with the exact DMRG results (see [39] for a discussion and [15] for a similar analysis of the continuum case).

Turning now to the question of pair correlations in the trapped system, Fig. 14.8 shows the pairs' MDF for a trapped Fermi gas: similar to the homogeneous case, a finite-momentum instability emerges upon polarizing the system. In order to verify the relation Eq. 14.12 in the trapped case, one has to take into account that for $P > P_c$, part of the total polarization goes into the fully polarized wings. In other words, the FFLO correlations are driven by a smaller effective polarization $P_{\text{eff}} < P$. In order to extract $P_{\text{eff}} < P$, we explain the strategy of [13]: the spatial extension L_{eff} of the quasi-condensate can be extracted by computing the highest occupied natural orbital ϕ_0 of the matrix ρ_{ij}^{pair} Eq. 14.11 (i.e., the eigenvector corresponding to the largest eigenvalue). An example for the spatial form of $|\phi_0|^2$, taken from [13], is shown in Fig. 14.7, which yields an illustration of the node structure in the 1D FFLO state. Note that the spin density takes maxima in the nodes of the quasi-condensate [44] (an analogous result for the spin density was obtained with QMC for the continuum case [15]).

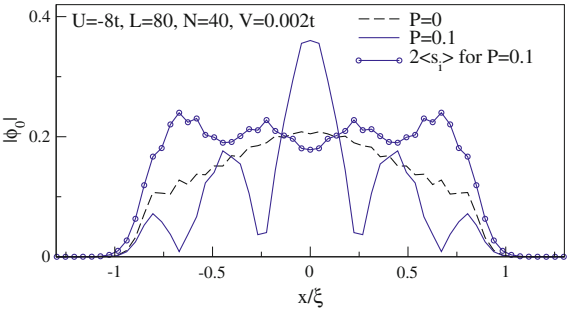

Fig. 14.7 Highest occupied natural orbital $|\phi_0|$ of a trapped 1D Fermi gas in an optical lattice for $P = 0, 0.1$ and $U = -8t$ (*lines*). The spin density is displayed with stars. The natural orbital yields a visualization of the 1D FFLO quasi-condensate. DMRG data taken from [13]

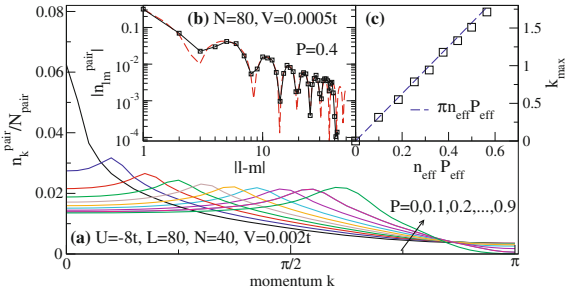

Fig. 14.8 **a** Momentum distribution function of pairs of a trapped, two-component Fermi gas with $U = -8t$ (see the legends for further parameters) described by the Hamiltonian Eq. 14.18. **b** Decay of pair correlations in real space and comparison of DMRG results (symbols) to the prediction from bosonization [12], Eq. 14.13 (*lines*). **c** The position of the maximum in n_k^{pair} shows the expected scaling with $Q = k_{F\uparrow} - k_{F\downarrow} = \pi n_{\text{eff}} P_{\text{eff}}$, where P_{eff} is the effective polarization in the partially polarized core (see the discussion in [13]). Reproduced from [13]

The effective polarization is then obtained by integrating $\langle s_i \rangle = \langle n_{i\uparrow} - n_{i\downarrow} \rangle$ over the spatial extent of $|\phi_0.|$ By plotting the position Q of the maximum in n_k^{pair} vs $n_{\text{eff}} P_{\text{eff}}$, one recovers the expected linear dependence in agreement with Eq. 14.12 (see Fig. 14.8c). Finally, the spatial decay of pair correlations at large $|U|$ indeed follows the prediction from bosonization, Eq. 14.13 [12], as we show in Fig. 14.8b.

Using DMRG, a variety of other correlation functions can be obtained as well in the partially polarized phase, including spin-spin correlations [17, 58], density-density correlations [17], and noise correlations [16]. The FFLO state leaves distinct fingerprints in these correlations and their respective Fourier transforms. For instance, the $2k_F$ peak/kink present in the structure factor for density-density correlations in the unpolarized case splits into two peaks at $2k_{F\uparrow}$ and $2k_{F\downarrow}$ [17]. The spin structure factor, as a consequence of the $2Q$ spin density wave that accompanies the FFLO state (see Fig. 14.7) has a pronounced kink at $2Q = 2(k_{F\uparrow} - k_{F\downarrow})$ [58]. A proposal

for the experimental measurement of spin correlations in a spin-polarized Fermi gas has been put forward in [58]. Finally, the FFLO correlations induce the presence of peaks in noise correlations whose distance is given by Q (for a detailed discussion, see [16]).

14.5 Spin- and Mass-Imbalanced Fermi Mixtures

So far we have discussed situations in which up and down fermions have the same mass (or effective mass) and are described by integrable models. In this section we address the more general problem in which pairing occurs between particles of different species, for example ^{6} Li and ^{40} K atoms [59–61]. In this case the masses of spin up and down fermions are different and the underlying Hamiltonian is no longer integrable. For lattice systems, the simplest model is the 1D asymmetric Fermi-Hubbard:

$$H = -\sum_{i\sigma} t_\sigma \left(c^\dagger_{i,\sigma} c_{i+1,\sigma} + h.c. \right) + U \sum_i n_{i\uparrow} n_{i\downarrow}, \tag{14.19}$$

where t_σ are spin-dependent tunneling rates. The model (14.19) has been studied recently by the bosonization method in [62], assuming equal densities of the two components, $n_\uparrow = n_\downarrow$. The extension to spin-imbalanced gases was first investigated numerically in [63, 64].

For equal masses, $t_\downarrow = t_\uparrow$, the exact solution of the Hubbard model shows that fermions can bind in pairs, but n-body bound states with $n > 2$ are generally forbidden. For unequal masses, it has recently been shown [65, 66] that three-body bound states, hereafter called trimers, exist and can considerably affect the many-body picture. Here we outline the key results of [65, 66].

The trimer gap, namely the energy needed to break a single trimer at finite density, is defined as

$$\Delta_{\rm tr} = -\lim_{L\to\infty} \Big[E_L(N_\uparrow + 1,\ N_\downarrow + 2) + E_L(N_\uparrow, N_\downarrow) - E_L(N_\uparrow + 1,\ N_\downarrow + 1) - E_L(N_\uparrow, N_\downarrow + 1) \Big], \tag{14.20}$$

where $E_L(N_\uparrow, N_\downarrow)$ is the ground state energy of a system with atom numbers $N_\uparrow$, $N_\downarrow$ in a chain of size L. The limit in Eq. 14.20 is taken assuming $N_\sigma \to \infty$ with $n_\sigma \equiv N_\sigma / L$ being fixed. Equation 14.20 has been evaluated by DMRG on lattices of up to $L = 160$ sites and the thermodynamic limit was extrapolated via finite-size scaling.

For equal masses, $t_\downarrow = t_\uparrow$, no trimers exist and therefore, $\Delta_{\rm tr} = 0$. For $t_\downarrow < t_\uparrow$, the trimer gap (14.20) is finite only when the two concentrations are commensurate, i.e., $n_\downarrow = 2n_\uparrow$. It is plotted in Fig. 14.9 as a function of $n_\downarrow$ and for different values of the interaction strength. We see that the gap is a decreasing function of the density

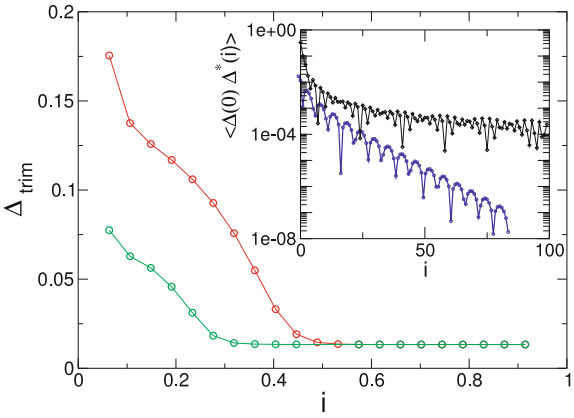

Fig. 14.9 Trimer energy gap (20) in unit of $t_\uparrow$ plotted versus density $n_\downarrow$ and different values of $U = -2t_\uparrow$ (bottom) and $U = -4t_\uparrow$. The mass anisotropy is $t_\downarrow = 0.3$. *Inset*: superconducting correlations as a function of the distance from the center of the chain for different values of the density $n_\downarrow = 0.7$ (upper curve), where $\Delta_{\rm tr} = 0$, *and* $n_\downarrow = 0.3$, where $\Delta_{\rm tr} > 0$. The parameters used are $U = -4t_\uparrow$, $t_\downarrow = 0.3t_\uparrow$ and $L = 200$ and the densities are commensurate, $n_\uparrow = n_\downarrow/2$. Notice the change from an algebraic to an exponential decay. Reproduced from [66]

and vanishes at a critical concentration $n_\downarrow = n_\downarrow^{\rm cr}$—in sharp contrast with the case of equal densities, $n_\uparrow = n_\downarrow$, where the associated pairing gap is *always* positive for any filling. This result is consistent with the bosonization analysis performed in [65]. In particular, for densities satisfying the constraint $pn_\uparrow - qn_\downarrow = 0$, with p, q integer numbers, the bosonized action includes the following interaction term

$$H_{\rm int} = A \int \cos 2(p\phi_\uparrow(z) - q\phi_\downarrow(z)), \tag{14.21}$$

where A is an amplitude and $\phi_\sigma(z)$ the phase operator of each component. For $p = q = 1$, the operator (14.21) describes pair superconductivity and is a relevant perturbation, implying that the pairing gap opens at any $U < 0$. For trimers, corresponding to $p = 1, q = 2$, the perturbation (14.21) is instead irrelevant, and the trimer gap only opens beyond a critical interaction strength, $U < U_c < 0$ or, equivalently, only at sufficiently low density.

The phase with $\Delta_{\rm tr} \neq 0$ corresponds to a Luttinger liquid of trimers. Since pairs are bound into these composite objects and cannot propagate freely, the long distance behavior of the superconducting FFLO correlations changes from algebraic to exponential decay, as shown in the inset of Fig. 14.9.

Next, we discuss the grand-canonical phase diagram of the asymmetric Hubbard model, which is obtained by replacing the densities $n_\uparrow$ and $n_\downarrow$ by two new variables, corresponding to the mean chemical potential $\mu = \partial E/\partial(N_\uparrow + N_\downarrow)$ and the *effective* magnetic field $h = \partial E/\partial(N_\uparrow - N_\downarrow)$, where E is the ground state energy calculated by DMRG. This is shown in Fig. 14.10, for fixed parameters $t_\downarrow/t_\uparrow = 0.3$ and $U = -4t_\uparrow$.

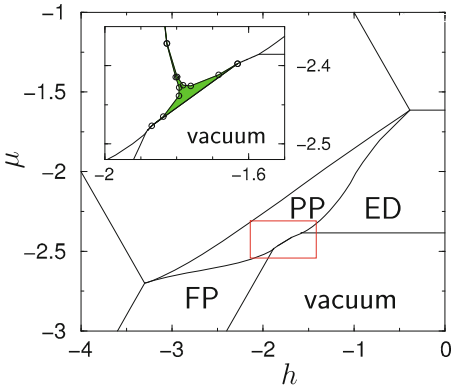

Fig. 14.10 Phase diagram of the asymmetric Hubbard model for $t_\downarrow = 0.3t_\uparrow$ and $U = -4t_\uparrow$. The novel line boundary between partially polarized phase and vacuum is a consequence of the existence of n-body bound states with $n > 2$. Inset: a zoom-in of the low density region of the PP phase. The locus of commensurate densities $n_\uparrow = n_\downarrow/2$ is shown by the shaded area. Reproduced from [66]

For clarity, only the $h < 0$ part of the phase diagram is displayed, corresponding to a majority of heavy ($\downarrow$) fermions.

The evolution of the overall shape of the phase diagram with changing $t_\downarrow$ has been presented in [64]. Here we concentrate on the topological changes induced by trimers. In particular, the boundary with the vacuum is given by the formula

$$\mu_{vac} = \min_{p,q} \frac{E(p,q) - (p-q)h}{p+q}, \tag{14.22}$$

where p, q are non negative integers and the size of the chain is sufficiently large. At the integrable point, where no trimer exists, the boundary (14.22) reduces to two lines, $E(0,1) - \mu + h = 0$ and $E(1,1) - 2\mu = 0$, separating the vacuum from the fully polarized (FP) and fully paired (ED) phases, respectively. The existence of additional bound states in the asymmetric Hubbard model implies that the partially polarized phase (PP) has a direct line boundary with the vacuum, as shown in Fig. 14.10. In particular, trimers are represented by the line $E(1,2) - 3\mu + h = 0$.

It is also instructive to consider the locus of $n_\uparrow = n_\downarrow/2$ on the phase diagram. At low density ($n_\downarrow < n_\downarrow^{\rm cr}$), the trimer gap is non-zero and the locus corresponds to the shaded area in the inset of Fig. 14.10. At higher density ($n_\downarrow > n_\downarrow^{\rm cr}$), the energy gap closes and the locus shrinks to a single line.

Finally, we would like to mention that trimers, though of a different origin, appear also in three-component Fermi gases [67–70] and in Bose gases [71, 72], leading to equally interesting many-body effects.

14.6 A Two-Channel Model: The Bose-Fermi Resonance Model

The previous sections focussed on one-channel models, i.e., attractively interacting fermions described by either the Gaudin–Yang model Eq. 14.1 or the 1D Hubbard model Eq. 14.16. Several aspects of the one-dimensional BCS–BEC crossover, though, cannot be captured by one-channel models. First, in the BEC limit, such models result in a Tonks–Girardeau gas of dimers. Therefore, the regime of weakly interacting bosons, which is reached when the characteristic length scale of the two-body bound state is smaller than the transverse oscillator length, is not captured. Second, models of attractively interacting fermions, in the case of a population imbalance, always feature the 1D FFLO state, for any interaction strength. In reality, both close to and beyond resonance, i.e., upon entering the BEC regime, minority fermions get bound into closed-channel molecules, and are thus not available anymore for pairing that would result in the FFLO state. Therefore, one expects a competition between the FFLO phase, stable on the BCS side, with a Bose-Fermi mixture in which the bosons are composite molecules in the closed channel, immersed into a fully polarized gas of fermions.

This second aspect can be incorporated in the framework of the so-called Bose-Fermi resonance (BFRM) model [73, 74]:

$$\hat{H}' = \hat{H} - \mu\hat{N} = \int dx \Big(\sum_{\sigma=\uparrow,\downarrow} \hat{\psi}_\sigma^\dagger \Big[-\frac{\hbar^2}{2m}\partial_x^2 - \mu \Big] \hat{\psi}_\sigma + \hat{\psi}_B^\dagger \Big[-\frac{\hbar^2}{4m}\partial_x^2 - 2\mu + \nu \Big] \hat{\psi}_B + g\left(\hat{\psi}_B^\dagger \hat{\psi}_\uparrow \hat{\psi}_\downarrow + h.c. \right) \Big) \tag{14.23}$$

where $\hat{\psi}_\sigma(x)$ (resp. $\hat{\psi}_B(x)$) are fermionic (resp. bosonic) field operators describing atoms (resp. the bound state in the closed channel, i.e., bare dimers), μ is the chemical potential, m (resp. $2m$) is the mass of the atoms (resp. of the bare dimers), ν is the detuning in energy of one bare dimer with respect to two atoms and g is the coupling constant for the conversion of two atoms into a bare dimer and vice-versa. In principle, there is also a direct background interaction between fermions of opposite spin. Our key interest here is in the behavior close to resonance, where the interactions mediated by the Feshbach coupling g dominate any background interaction. For a negative detuning $\nu < 0$ of the molecular level, g gives rise to an attractive two-particle interaction $g^2/\nu < 0$ between the fermions [34].

An important insight into the properties of the BCS–BEC crossover of a spin imbalanced gas in 1D was gained by Baur et al. [75], who studied the associated three-body problem. In the Sec. 14.2, we pointed out that the BCS–BEC crossover of a balanced Fermi gas is smooth. This changes once one goes to a finite imbalance, which can be captured already on the three-body level, as pointed out by Baur et al. [75]. By writing the wave function as

$$|\psi\rangle = \left(\sum_K f_K b_K^\dagger c_{-K}^\dagger + \sum_{k,K} g_{k,K} c_{K\downarrow}^\dagger c_{k-K/2\uparrow} c_{-k-K/2\uparrow} |0\rangle \right) \tag{14.24}$$

where $b_K^\dagger$ creates a molecule with momentum K, one can show that the function f_K is either symmetric, namely on the BEC side, or antisymmetric, namely on the BCS side, upon exchanging the position of the molecule and the fermion [75]. This change in the symmetry of the wave-function occurs at $v' = v/g^{4/3} \approx 0.635$, i.e., on the BEC side of the resonance, and can be traced back to a level-crossing of the symmetric and anti-symmetric wave-functions [75]. Baur et al. further used Quantum Monto Carlo simulations to compute the thermal density matrix on the three-body level, finding results consistent with their analytical predictions.

14.6.1 Phase Diagram of the Bose-Fermi Resonance Model at Finite Imbalance

The analytical results by Baur et al. suggest that a phase transition could be present in the many-body case at a finite imbalance, separating the FFLO phase from a Bose-Fermi mixture. Such a transition would eventually be characterized by a complete depletion of the minority fermions and consequently, the corresponding Fermi volume vanishes. A general discussion of the possible phases along the crossover depending on the number of Fermi surfaces is given in [76].

The BFRM, unlike the one-channel model discussed before, does not allow for an analytically exact solution. One therefore has to resort to numerical approaches, which in one dimension can still provide us with exact results. In the present case, DMRG can be applied, yet it requires a discretization of the model (14.23). Thus, we rewrite the Hamiltonian in a real-space version:

$$\begin{aligned} H = & -t \sum_{i=1}^{L-1} (c_{i,\sigma}^\dagger c_{i+1,\sigma} + h.c.) \\ & - t_{\text{mol}} \sum_{i=1}^{L-1} (m_i^\dagger m_{i+1} + h.c.) - (v + 3t) \sum_{i=1}^{L} m_i^\dagger m_i \\ & + g \sum_{i=1}^{L} (m_i^\dagger c_{i,\uparrow} c_{i,\downarrow} + h.c.). \end{aligned} \tag{14.25}$$

Here, $m_i^\dagger$ creates a composite boson on site i. The boson energy is shifted with respect to that of single fermions by an effective detuning $v + 3t$. It is chosen such that the energies for adding two fermions or one boson, each at zero momentum, coincide at resonance $v = 0$. The hopping matrix elements for fermions and molecules are denoted by t and $t_{\text{mol}} = t/2$, respectively. The only conserved particle number is

$N = N_f + 2N_{\rm mol}$, where $N_{\rm mol} = \sum_i \langle n_i^{\rm mol} \rangle$; $n_i^{\rm mol} = m_i^\dagger m_i$ and $N_f = N_\uparrow + N_\downarrow$. We use $n = N/L$ to denote the filling factor. Note that at maximum one molecule can sit on a single site, *i.e.*, the molecules behave as hard-core bosons.

The phase diagram can be obtained by calculating various quantities, including the MDF of pairs, molecules and the fermionic components, as well as polarization curves and the density in the molecular channel as a function of polarization P and detuning v. While details on such calculations are given in [19], we here wish to focus on the discussion of the emergent phases. A typical phase diagram is shown in Fig. 14.11a as magnetic field $h' = h/\varepsilon^*$ versus dimensionless detuning $v' = v/\varepsilon^*$. h is defined as the difference in chemical potential for spin up and down while ε^* is the binding energy at resonance $v = 0$ [19]. For $h' < h_c$, the system remains balanced, and we thus recover the BCS–BEC crossover of a balanced mixture, discussed in Sec. 14.2. For $h' > h_{\rm sat}$, the system is fully polarized with $n_\uparrow = n$. As expected, the FFLO phase is stable on the BCS side in the imbalanced case $h_c < h'$. The system then undergoes two consecutive phase transitions, either at a fixed polarization $P > 0$ or at a fixed detuning in the vicinity of the resonance $v' \lesssim 0$, at two critical fields h_1 and h_2. The phase boundary of the FFLO phase is given by $h' = h_1(v')$ [19], or by $P = P_1'(v')$, respectively. The intermediate phase, labeled *BEC + PP LL* (BEC plus partially polarized Luttinger liquid), still has oscillatory correlations, yet there are instabilities in the pairs' MDF at both finite and zero momentum [19]. While in the FFLO and in the *BEC + PP LL* phase, $n_\downarrow > 0$, the transition into the Bose-Fermi mixture phase *BEC + FP FG* (BEC plus fully polarized Fermi gas) occurs at the point at which $n_\downarrow = 0$ [19]. The *BEC + FP FG* has smooth algebraically decaying dimer-dimer correlations (and consequently, pair-pair correlations), with no oscillatory component. Note that in a one-channel model, in contrast to the BFRM, the line with $n_\downarrow = 0$ is equivalent to full polarization $n = n_\uparrow$. Therefore, the upper limit for the stability of the FFLO state is the maximum polarization possible, suggesting that FFLO is more stable in one-channel models (compare the discussion in Sect. 14.4).

In the example shown here ($g = t$, filling $n = 0.6$), the FFLO phase breaks down before resonance $v' < 0$ on the BCS side and the phase boundary exhibits a significant dependence on polarization. In general, the critical detuning, which is the detuning at which FFLO correlations disappear in the $P \to 0$ limit, depends on both the filling and the Feshbach coupling g. For instance, at a fixed value of g, sending the density to zero moves the phase boundary towards larger v'. In the example shown in the figure, the critical detuning, approaches $v' \approx 0.97$ as $n \to 0$ [19], which is beyond resonance on the BEC side, consistent with the results by Baur et al. for the associated three-body problem in the continuum [75].

So far we have not specified a specific realization of the model (14.23) since we have treated v and g as model parameters. It could, for instance, model a resonance due to photoassociation or a confinement-induced resonance (see the discussion in [34]). To allow a discussion of the phase diagram in terms of experimentally accessible parameters, it is useful to replace the detuning v' by the parameter $\gamma = \sqrt{\varepsilon_b(v')/\varepsilon_F}$ where $\varepsilon_b(v)$ is the two-body binding energy and $\varepsilon_F = 2t(1 - \cos(k_F))$ is the Fermi energy of a noninteracting gas at the same density. In the continuum limit, this yields the usual definition of the interaction parameter γ. The corresponding behavior

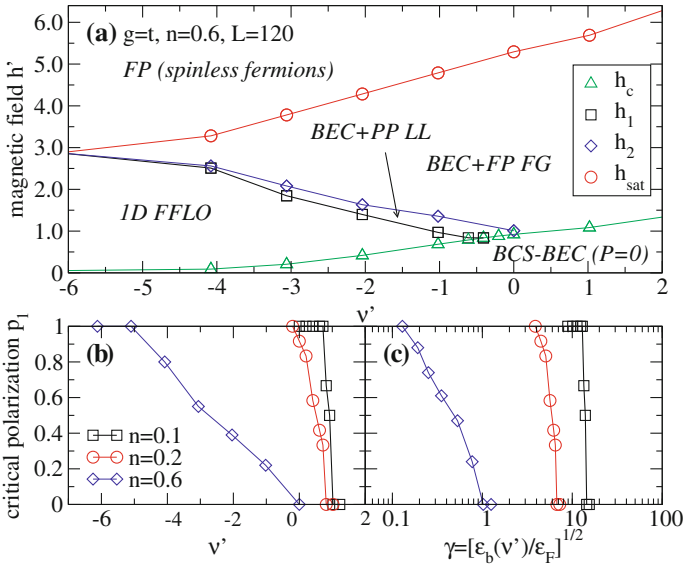

Fig. 14.11 Phase diagram of the Bose-Fermi resonance model Eq. 14.25 for $g = t$: **a** Dimensionless field h' vs dimensionless detuning ν'. **b** Critical polarization P_1 vs detuning ν' for $n = 0.1, 0.2, 0.6$. **c** Critical polarization P_1 vs ratio of binding energy over Fermi energy $\gamma = \sqrt{\varepsilon_b/\varepsilon_F}$. Figures reproduced from [19]

is displayed in Fig. 14.11c as a polarization vs. γ phase diagram. We only show the phase boundary $P = P_1$ (corresponding to $h' = h_1$) of the 1D FFLO phase, for different densities n. Obviously, for a given n, the ratio of binding energy over Fermi energy determines the range of stability for FFLO. By decreasing n at a fixed g, FFLO becomes stable at arbitrarily large values of γ.

Finally, we emphasize that the limit of a broad resonance, characterized by $nr^* \ll 1$ (compare the discussion of Sec. 14.2) can be reached by either decreasing density or by increasing g such that the binding energy at resonance $\varepsilon_b^* = \varepsilon_b(v = 0)$ increases. For the parameters of Fig. 14.11a ($g = t$, $n = 0.6$), the system is not in this regime since $nr^* \approx 1.21$, yet enters into this limit as n decreases (compare Fig. 14.11b, c).

14.7 Beyond 1D, Other Variations

The FFLO phase occupies a tiny sliver of the $T = 0$ phase diagram in three dimensions and this region shrinks with increasing temperature, making it very difficult for the experimentalist to detect it. In one dimension, on the contrary, nesting effects are pervasive at all fillings and polarization, the FFLO instability becomes enhanced, and the phase more robust. In experiments with cold atoms, low dimensions are now

within reach [1, 8, 9], paving the way to its realization. Strictly in one dimension, the FFLO phase occupies large regions of the phase diagram as we have illustrated in this chapter.

Even though the FFLO phase is more robust in 1D, long-range order is not present, and one can only describe a *quasi* long-range order with algebraically decaying correlations. Moreover, in order to realize this physics one should effectively be able to reach zero temperature. However, this obstacle can be remedied in part by turning on a weak coupling between 1D chains. Cold atoms experiments are carried out by loading the fermions onto 1D tubes, formed by the interference pattern of sets of counter-propagating lasers. By tuning the intensity of the lasers one could adiabatically turn on the coupling between the tubes, allowing one to study the dimensional crossover from 1D to 3D (or 2D) [51, 77]. Unfortunately, this scenario is out of reach for DMRG (at least as far as the crossover from 1D to 3D is concerned) and has so far only been studied within an effective field theory [51], by a mean-field treatment [77], or by feeding in the exactly known instabilities of the 1D system into an RPA analysis [16]. Both approaches [16, 51] show that depending on polarization, interaction strength, and inter-tube coupling, the system is either in the FFLO phase or becomes a polarized Fermi liquid. In [77] the authors raised the possibility of finding two distinct FFLO phases as one increases the tunneling between chains: In a 1D system and within a mean-field description, the order parameter possesses nodes, or domain walls, resembling a soliton-like structure, with the excess fermions concentrated at these nodes. One can imagine coupling chains into a higher dimensional array. The excess Fermions would feel the soliton structure as a superimposed lattice and will form a band of Andreev bound states that is filled, similar to a band insulator. This phase is called a commensurate FFLO phase in [77]. A plausible scenario is that at intermediate inter-chain couplings, the system could undergo a transition to an incommensurate FFLO phase where the band of Andreev bound states is partially filled. This is a mean-field scenario that has not been further explored.

An alternative path was taken in [78]. A "poor man's" version of the dimensional crossover could be achieved by arranging the tubes into a super-lattice, coupling pairs of them into ladders (basically two one-dimensional chains coupled in the transverse direction). Interestingly enough, most of the two-dimensional physics already manifests itself in these systems: At low densities only one band is occupied for each flavor of spin, and the physics reduces to the that of one dimension. This in turn can be associated to the rotational symmetric situation in higher dimensions, in which the Fermi surfaces are spheres, and the order parameter can be described by a single wave vector $|\mathbf{Q}|$. As the density is increased, more bands start being occupied, and multiple Fermi points contribute to pairing. As a consequence, a multi-nodal FFLO order parameter is required to describe the new scenario. The ladder geometry is still highly nested, making the FFLO phase very robust. However, in two dimensions, particularly at high densities or magnetic fields, the nesting between bands with opposite spin is weak, with Fermi surfaces with different shapes, and large mismatch in Fermi velocities. This makes pairing—and the FFLO state—unfavorable, giving room for a normal polarized phase.

As discussed in earlier sections, in a trapped gas in 3D and also in 2D [79], the partially polarized phase and thus the FFLO phase is in the core of the trapped cloud, according to mean-field calculations. This behavior can already be seen on the two-leg geometry at small polarizations [78], suggesting this one as a useful toy system to understand aspects of the dimensional crossover in a model that allows for a numerically exact solution.

An additional motivation for studying the attractive Hubbard model comes from the fact that the knowledge on the phases of the spin-imbalanced, attractive model also gives information on the ground states of the repulsive model via a particle-hole transformation. This could become relevant for 2D systems where in general, the ground states are not known, calling for experiments in this direction (see the discussion in [80, 81]).

Interesting possibilities arise when multi-band pairing is considered [82]. Consider a setup with anisotropic Fermi surfaces, in which the tunnelling along the x direction is much weaker than the other two (transverse) directions. This leads to a multi-band scenario in which one spin species populates only the s-band, while the other partially occupies the p_x band directly above, with Fermi surfaces lying on different bands. This gives rise to a new unconventional FFLO-like paired state, with the main difference that the pairs have p-wave center-of-mass momenta, and an order parameter modulated by a wave-vector $\mathbf{Q} = \mathbf{k}_F^{\uparrow} + \mathbf{k}_F^{\downarrow}$.

Remarkably, optical lattices can potentially be tuned independently for both hyperfine species [83]. This technique could provide another knob for tuning their relative masses, or changing the shape and relative orientation of the Fermi surfaces. For instance, in [84], the authors proposed rotating the Fermi surfaces for each spin flavor by 90 degrees with respect to one another. Then, FFLO-like physics with a modulated order parameter can be realized in *unpolarized* mixtures. A similar idea has been discussed to realize exotic unpolarized phases in 1D, using a multi-band setup [85].

Other authors [70, 86–90] have also considered multi-flavor systems, in which three hyperfine species are present, interacting via attractive interactions. This gives rise to a rich variety of possibilities beyond FFLO, such as molecules (trions), and a competition between three pairing tendencies with different center-of-mass momenta. Moreover, the BCS–BEC crossover of a balanced mixture of a four-component gas has recently been discussed in [91]. Finally, FFLO-like phases can also be stable in the case of repulsive interactions on the ladder geometry [92, 93].

14.8 Proposals for the Experimental Observation of FFLO Correlations

One of the main open experimental challenges is the actual characterization of the partially polarized phase as the FFLO phase. While the phase-separated profiles observed in the Rice experiment [8] show a remarkable agreement with the theoretical

predictions obtained from the Bethe ansatz combined with LDA [6, 7], experiments have not unambiguously demonstrated that the phase indeed corresponds to a paired state with a finite center-of-mass momentum. This is not a trivial task, since the number of available techniques to probe cold atomic systems remains limited. However, the quest for the FFLO state has certainly presented an extraordinary motivation and the breeding ground for novel and clever ideas. The most straightforward possibility is to take snapshots trying to resolve the spin density modulations [13, 15, 44]. Another possibility is to probe the spin–spin correlations using spatially resolved quantum polarization spectroscopy [58]. While the spin modulations are characteristic of the FFLO state, they are no direct evidence of pairing. One way to identify pairing may be using a time-of-flight (TOF) measurement to observe the velocity distribution of the condensate. Since the pairs have finite center-of-mass momenta, they would imprint a characteristic signature [94].

The latter work also has proposed to use noise correlations, and mean-field [95] and DMRG studies [16] show that this technique would indeed produce a clear and unambiguous signal. Although spectroscopic techniques to probe cold atomic systems are under development and are not widely available [96], FFLO signatures should also be evident in the rf-spectra [97, 98] and angle resolved photo-emission spectra [84]. An interesting recent proposal consists of studying the response of the system to time-dependent potentials [99], which would excite the spin-dipole modes. When the oscillation of the potential is in resonance with the excitations, a dramatic response at the proper momenta would indicate FFLO physics. Another idea exploiting time-dependent perturbations using modulation spectroscopy [100] consists of measuring the response of the double occupancy [101]. At present, the only relevant experiment is the one by Yiao et al. [8], which realizes 1D tubes in the continuum. Therefore, for this particular system, proposals that assume the presence of an optical lattice along the 1D direction may not be applicable [101]. It should further be stressed that some of the ideas put forward here have only been substantiated by mean-field theory [95, 97, 99]. While one may argue that mean-field theory gives qualitatively reasonable results for the phase diagram of attractively interacting fermions in 1D [22, 102], there are considerable quantitative deficiencies already on the level of density profiles [98] and it is by no means obvious that mean-field theory is valid for the description of time-dependent detection schemes [97, 99].

Finally, for the question of whether FFLO can be observed in an actual experiment, the accessible temperatures may play a crucial role [15, 37, 103, 104]. The effect of temperature on density profiles in traps was studied with Bethe-ansatz methods in [37] and numerically using QMC in [15, 104]. In [104], the visibility of the finite-momentum peak in the pairs' MDF was also discussed as a function of temperature.

In conclusion, while all these ideas can potentially provide the smoking gun that would signal the presence of the FFLO phase in experiments, their implementation still remains challenging, and some have shortcomings. However, it is very likely that some of these techniques may routinely be used in the future.

14.9 Summary

The recent realization of 1D Fermi gases with ultracold atoms in the vicinity of a Feshbach resonance [8] opens the possibility to investigate the physics of strongly correlated fermions in a situation, where exact analytical or numerical results are available. As shown above, this makes accessible the physics of solvable models such as those of Gaudin, Yang, Lieb and Wu and others. It also provides a means to study unconventional pairing of the FFLO-type in a simple example. Compared to the BCS–BEC crossover in 3D, where a number of open questions still exists for the imbalanced gas, the 1D case is rather well understood, at least as far as equilibrium quantities are concerned. Issues such as equilibration or the expansion dynamics, or the effects of finite temperature are, however, still open and topics of ongoing research. The physics of 1D fermions will thus remain of interest for some time to come, in particular, because ultracold atoms provide an experimental realization that allows one to investigate physics in one dimension over a wide range of parameters.

Acknowledgments F.H.-M. and W.Z. acknowledge support from the Deutsche Forschungsgemeinschaft through FOR801. A.E.F. acknowledges support from the NSF through grant DMR-0955707. We thank R. Hulet for very fruitful discussions.

References

1. Bloch, I., Dalibard, J., Zwerger, W.: Rev. Mod. Phys. **80**, 885 (2008)
2. Giorgini, S., Pitaevskii, L.P., Stringari, S.: Rev. Mod. Phys. **80**, 1215 (2009)
3. Ketterle, W., Zwierlein, M.: In: Inguscio, M. (ed.) Ultracold Fermi Gases, Proceedings of the International School of Physics "Enrico Fermi", Course CLXIV, Varenna, 20–30 June 2006, (2008)
4. Fuchs, J.N., Recati, A., Zwerger, W.: Phys. Rev. Lett. **93**, 090408 (2004)
5. Tokatly, I.V.: Phys. Rev. Lett. **93**, 090405 (2004)
6. Hu, H., Liu, X.J., Drummond, P.D.: Phys. Rev. Lett. **98**, 070403 (2007)
7. Orso, G.: Phys. Rev. Lett. **98**, 070402 (2007)
8. Liao, Y.A., Rittner, A.S.C., Paprotta, T., Li, W., Partridge, G.B., Hulet, R.G., Baur, S.K., Mueller, E.J.: Nature **467**, 567 (2010)
9. Moritz, H., Stöferle, T., Günter, K., Köhl, M., Esslinger, T.: Phys. Rev. Lett. **94**, 210401 (2005)
10. Fulde, P., Ferrell, A.: Phys. Rev. **135**, A550 (1964)
11. Larkin, A., Ovchinnikov, Y.: Zh. Eksp. Teor. Fiz. **47**, 1136 (1964)
12. Yang, K.: Phys. Rev. B **63**, 140511 (2001)
13. Feiguin, A., Heidrich-Meisner, F.: Phys. Rev. B **76**, 220508(R) (2007)
14. Batrouni, G.G., Huntley, M.H., Rousseau, V.G., Scalettar, R.T.: Phys. Rev. Lett. **100**, 116405 (2008)
15. Casula, M., Ceperley, D.M., Mueller, E.J.: Phys. Rev. A **78**, 033607 (2008)
16. Lüscher, A., Noack, R., Läuchli, A.: Phys. Rev. A **78**, 013637 (2008)
17. Rizzi, M., Polini, M., Cazalilla, M., Bakhtiari, M., Tosi, M., Fazio, R.: Phys. Rev. B **77**, 245105 (2008)
18. Tezuka, M., Ueda, M.: Phys. Rev. Lett. **100**, 110403 (2008)
19. Heidrich-Meisner, F., Feiguin, A.E., Schollwöck, U., Zwerger, W.: Phys. Rev. A **81**(023629), 023629 (2010)

20. Casalbuoni, R., Nardulli, G.: Rev. Mod. Phys. **76**, 263 (2004)
21. Lortz, R., Wang, Y., Demuer, A., Böttger, P.H.M., Bergk, B., Zwicknagl, G., Nakazawa, Y., Wosnitza, J.: Phys. Rev. Lett. **99**, 187002 (2007)
22. Sheehy, D.E., Radzihovsky, L.: Ann. Phys. **322**, 1790 (2007)
23. Radzihovsky, L., Sheehy, D.: Rep. Prog. Phys. **73**, 076501 (2010)
24. Randeria, M., Duan, J.M., Shieh, L.Y.: Phys. Rev. Lett. **62**, 98 (1989)
25. Olshanii, M.: Phys. Rev. Lett. **81**, 938 (1998)
26. Gaudin, M.M.: Phys. Lett. **24A**, 55 (1967)
27. Yang, C.N.: Phys. Rev. Lett. **19**, 1312 (1967)
28. Bergeman, T., Moore, M.G., Olshanii, M.: Phys. Rev. Lett. **91**, 163201 (2003)
29. Mora, C., Egger, R., Gogolin, A.O.: Phys. Rev. A **71**, 052705 (2005)
30. Petrov, D.S.: Phys. Rev. A **67**, 010703 (2003)
31. Lieb, E.: Phys. Rev. **130**, 1605 (1963)
32. Giamarchi, T., Nattermann, T., LeDoussal, P.: Fundamental problems of mesoscopic physics. Nato Science Series II **154**, 275 (2004)
33. Luther, A., Peschel, I.: Phys. Rev. B **74**, 002911 (1974)
34. Recati, A., Fuchs, J., Zwerger, W.: Phys. Rev. A **71**, 033630 (2005)
35. Citro, R., Orignac, E.: Phys. Rev. Lett. **95**, 130402 (2005)
36. Sheehy, D.E., Radzihovsky, L.: Phys. Rev. Lett. **95**, 130401 (2005)
37. Kakashvili, P., Bolech, C.J.: Phys. Rev. A **79**, 041603 (2009)
38. Zhao, E., Guan, X.W., Liu, W.V., Batchelor, M.T., Oshikawa, M.: Phys. Rev. Lett. **103**, 140404 (2009)
39. Heidrich-Meisner, F., Orso, G., Feiguin, A.E.: Phys. Rev. A **81**, 053602 (2010)
40. Silva, T.N.D., Mueller, E.J.: Phys. Rev. A **73**, 051602 (2006)
41. Woynarovich, F., Eckle, H., Trunng, T.: J. Phys. A Math. Gen. **22**, 4207 (1989)
42. Guan, X.W., Batchelor, M.T., Lee, C., Bortz, M.: Phys. Rev. B **76**, 085120 (2007)
43. Buzdin, A.I., Tugushev, V.V.: Zh. Eksp. Teor. Fiz. **85**, 735 (1983)
44. Machida, K., Nakanishi, H.: Phys. Rev. B **30**, 122 (1984)
45. Frahm, H., Korepin, V.E.: Phys. Rev. B **42**, 10553 (1990)
46. Frahm, H., Korepin, V.E.: Phys. Rev. B **43**, 56532 (1991)
47. Pokrovsky, V.L., Talapov, A.L.: Phys. Rev. Lett. **42**, 65 (1979)
48. Feiguin, A.E., Huse, D.A.: Phys. Rev. B **79**, 100507(R) (2009)
49. Frahm, H., Vekua, T.: J. Stat. Mech. P01007 (2008)
50. Vekua, T., Matveenkov, S., Shlyapnikov, G.: JETP Lett. **90**, 289 (2009)
51. Zhao, E., Liu, W.V.: Phys. Rev. A **78**, 063605 (2008)
52. McGuire, J.B.: J. Math. Phys. **7**, 123 (1965)
53. He, J., Foerster, A., Guan, X., Batchelor, M.T.: New J. Phys. **11**, 073009 (2009)
54. Essler, F., Frahm, H., Göhmann, F., Klümper, A., Korepin, V.E.: The One-Dimensional Hubbard Model. Cambridge University Press, Cambridge (2005)
55. Schollwöck, U.: Rev. Mod. Phys. **77**, 259 (2005)
56. White, S.R.: Phys. Rev. Lett. **69**, 2863 (1992)
57. Tezuka, M., Ueda, M.: New J. Phys. **12**, 055029 (2010)
58. Roscilde, T., Rodriguez, M., Eckert, K., Romero-Isart, O., Lewenstein, M., Polzik, E., Sanpera, A.: New J. Phys. **11**, 055041 (2009)
59. Wille, E., Spiegelhalder, F.M., Kerner, G., Naik, D., Trenkwalder, A., Hendl, G., Schreck, F., Grimm, R., Tiecke, T.G., Walraven, J.T.M., Kokkelmans, S.J.J.M.F., Tiesinga, E., Julienne, P.S.: Phys. Rev. Lett. **100**, 053201 (2008)
60. Voigt, A.C., Taglieber, M., Costa, L., Aoki, T., Wieser, W., Hänsch, T.W., Dieckmann, K.: Phys. Rev. Lett. **102**, 020405 (2009)
61. Orso, G., Pitaevskii, L.P., Stringari, S.: Phys. Rev. A **77**, 033611 (2008)
62. Cazalilla, M.A., Ho, A.F., Giamarchi, T.: Phys. Rev. Lett. **95**, 226402 (2005)
63. Batrouni, G.G., Wolak, M.J., Hebert, F., Rousseau, V.G.: EPL **86**, 47006 (2009)
64. Wang, B., Chen, H.D., Sarma, S.D.: Phys. Rev. A **79**, 051604(R) (2009)

65. Burovski, E., Orso, G., Jolicoeur, T.: Phys. Rev. Lett. **103**, 215301 (2009)
66. Orso, G., Burovski, E., Jolicoeur, T.: Phys. Rev. Lett. **104**, 065301 (2010)
67. Azaria, P., Capponi, S., Lecheminant, P.: Phys. Rev. A **80**, 041604 (2009)
68. Guan, X.W., Batchelor, M.T., Lee, C., Zhou, H.-Q.: Phys. Rev. Lett. **100**, 200401 (2008)
69. Kantian, A., Dalmonte, M., Diehl, S., Hofstetter, W., Zoller, P., Daley, A.J.: Phys. Rev. Lett. **103**, 240401 (2009)
70. Lüscher, A., Läuchli, A. arXiv:0906.0768 (unpublished)
71. Keilmann, T., Cirac, I., Roscilde, T.: Phys. Rev. Lett. **102**, 255304 (2009)
72. Valiente, M., Petrosyan, D., Saenz, A.: Phys. Rev. A **81**, 011601 (2010)
73. Timmermans, E., Furuyab, K., Milonnia, P.W., Kermanc, A.K.: Phys. Lett. A **285**, 228 (2001)
74. Holland, M., Kokkelmans, S.J.J.M.F., Chiofalo, M.L., Walser, R.: Phys. Rev. Lett. **87**, 120406 (2001)
75. Baur, S.K., Shumway, J., Mueller, E.J.: Phys. Rev. A **81**, 033628 (2010)
76. Sachdev, S., Yang, K.: Phys. Rev. B **73**, 174504 (2006)
77. Parish, M.M., Baur, S.K., Mueller, E.J., Huse, D.A.: Phys. Rev. Lett. **99**, 250403 (2007)
78. Feiguin, A., Heidrich-Meisner, F.: Phys. Rev. Lett. **102**, 076403 (2009)
79. Conduit, G.J., Conlon, P.H., Simons, B.D.: Phys. Rev. A **77**, 053617 (2008)
80. Ho, A.F., Cazalilla, M.A., Giamarchi, T.: Phys. Rev. A **79**, 033620 (2009)
81. Moreo, A., Scalapino, D.J.: Phys. Rev. Lett. **98**, 216402 (2007)
82. Zhang, Z., Hung, H.H., Ho, C.M., Zhao, E., Liu, W.V.: Phys. Rev. A **82**, 033610 (2010)
83. Liu, W.V., Wilczek, F., Zoller, P.: Phys. Rev. A **70**, 033603 (2004)
84. Feiguin, A.E., Fisher, M.P.A.: Phys. Rev. Lett. **103**, 025303 (2009)
85. Zapata, I., Wunsch, B., Zinner, N.T., Demler, E.: Phys. Rev. Lett. **105**, 095301 (2010)
86. Cherng, R.W., Refael, G., Demler, E.: Phys. Rev. Lett. **99**, 130406 (2007)
87. Rapp, A., Zaránd, G., Honerkamp, C., Hofstetter, W.: Phys. Rev. Lett. **98**, 160405 (2007)
88. Capponi, S., Roux, G., Lecheminant, P., Azaria, P., Boulat, E., White, S.R.: Phys. Rev. A **77**, 013624 (2008)
89. Capponi, S., Roux, G., Azaria, P., Boulat, E., Lecheminant, P.: Phys. Rev. B **75**, 100503 (2007)
90. Roux, G., Capponi, S., Lecheminant, P., Azaria, P.: Eur. Phys. J. B **68**, 293 (2009)
91. Nishida, Y., Son, D.: Phys. Rev. A **82**, 043606 (2010)
92. Roux, G., White, S.R., Capponi, S., Poilblanc, D.: Phys. Rev. Lett. **97**, 087207 (2006)
93. Roux, G., Orignac, E., Pujol, P., Poilblanc, D.: Phys. Rev. B **75**, 245119 (2007)
94. Yang, K.: Phys. Rev. Lett. **95**, 218903 (2005)
95. Paananen, T., Koponen, T.K., Törmä, P., Martikainen, J.P.: Phys. Rev. A **77**, 053602 (2008)
96. Stewart, J., Gaebler, J., Jin, D.: Nature **454**, 744 (2008)
97. Bakhtiari, M.R., Leskinen, M.J., Törmä, P.: Phys. Rev. Lett. **101**, 120404 (2008)
98. Molina, R.A., Dukelsky, J., Schmitteckert, P.: Phys. Rev. Lett. **102**, 168901 (2009)
99. Edge, J.M., Cooper, N.R.: Phys. Rev. Lett. **103**, 065301 (2009)
100. Kollath, C., Iucci, A., Giamarchi, T., Hofstetter, W., Schollwöck, U.: Phys. Rev. Lett. **97**, 050402 (2006)
101. Korolyuk, A., Massel, F., Törma, P.: Phys. Rev. Lett. **104**, 236402 (2010)
102. Liu, X.J., Hu, H., Drummond, P.D.: Phys. Rev. A **75**, 023614 (2007)
103. Liu, X.J., Hu, H., Drummond, P.D.: Phys. Rev. A **76**, 043605 (2007)
104. Wolak, M.J., Rousseau, V.G., Miniatura, C., Gremaud, B., Scalettar, R.T., Batrouni, G.G.: Phys. Rev. A **82**, 013614 (2010)